



**UNIVERSITY OF LEEDS**

This is a repository copy of *A computational approach to an optimal partition problem on surfaces*.

White Rose Research Online URL for this paper:  
<http://eprints.whiterose.ac.uk/80115/>

---

**Article:**

Elliott, CM and Ranner, T (2014) A computational approach to an optimal partition problem on surfaces. (Unpublished)

---

**Reuse**

Unless indicated otherwise, fulltext items are protected by copyright with all rights reserved. The copyright exception in section 29 of the Copyright, Designs and Patents Act 1988 allows the making of a single copy solely for the purpose of non-commercial research or private study within the limits of fair dealing. The publisher or other rights-holder may allow further reproduction and re-use of this version - refer to the White Rose Research Online record for this item. Where records identify the publisher as the copyright holder, users can verify any specific terms of use on the publisher's website.

**Takedown**

If you consider content in White Rose Research Online to be in breach of UK law, please notify us by emailing [eprints@whiterose.ac.uk](mailto:eprints@whiterose.ac.uk) including the URL of the record and the reason for the withdrawal request.



[eprints@whiterose.ac.uk](mailto:eprints@whiterose.ac.uk)  
<https://eprints.whiterose.ac.uk/>

# A computational approach to an optimal partition problem on surfaces

Charles M. Elliott

Mathematics Institute, Zeeman Building, University of Warwick. CV4 7AL. UK.

C.M.Elliott@warwick.ac.uk

Thomas Ranner

School of Computing, EC Stoner Building, University of Leeds. LS2 9JT. UK.

T.Ranner@leeds.ac.uk

## Abstract

We explore an optimal partition problem on surfaces using a computational approach. The problem is to minimise the sum of the first Dirichlet Laplace–Beltrami operator eigenvalues over a given number of partitions of a surface. We consider a method based on eigenfunction segregation and perform calculations using modern high performance computing techniques. We first test the accuracy of the method in the case of three partitions on the sphere then explore the problem for higher numbers of partitions and on other surfaces.

*2010 Mathematics Subject Classification:* Primary 49Q10; Secondary 49R50, 35R01, 65M60.

*Keywords:* Optimal eigenvalue partition; Surface decomposition; Finite element methods.

## 1 Introduction

In this paper, we use the surface finite element method to tackle an eigenvalue optimal partition problem for  $n$ -dimensional hypersurfaces in  $\mathbb{R}^{n+1}$ . Our computations are restricted to  $n = 2$ . We denote by  $\Gamma$  a closed, smooth, connected  $n$ -dimensional hypersurface embedded in  $\mathbb{R}^{n+1}$ . For a given positive integer  $m$ , we say that  $\{\Gamma_i\}_{i=1}^m$  is an  $m$ -partition of  $\Gamma$  if  $\Gamma_i \subset \Gamma$  for  $i = 1, \dots, m$ ,  $\Gamma_i \cap \Gamma_j = \emptyset$  for  $i, j = 1, \dots, m$  with  $i \neq j$  and  $\bigcup_{i=1, \dots, m} \bar{\Gamma}_i = \Gamma$ .

**Problem 1.1.** Given a positive integer  $m$  and a smooth surface  $\Gamma$ , divide  $\Gamma$  into an  $m$ -partition  $\{\Gamma_i\}_{i=1}^m$  to minimise the energy:

$$\mathcal{E}(\{\Gamma_i\}_{i=1}^m) = \sum_{i=1}^m \lambda_1(\Gamma_i), \quad (1.1)$$

where  $\lambda_1(\Gamma_i)$  is the first eigenvalue of the Dirichlet Laplace–Beltrami operator over  $\Gamma_i$ .



This is a generalisation of a similar problem considered in various formulations over a Cartesian domain  $\Omega$  with appropriate boundary conditions. The flat problem was studied in the context of shape optimisation in the 1990's by Buttazzo and Dal Maso (1993); Sverak (1993); Bucur and Zolesio (1995); Bucur, Buttazzo and Henrot (1998). A key challenge is how to define an appropriate space of admissible partitions and how to equip this space with a topology so that one can define an absolute minimiser. By restricting to quasi-open sets, Bucur et al. (1998) show existence of an optimal partition as a consequence of a more general result. Quasi-open sets are sets which are close to open sets in the sense that given a quasi-open set there is an open set such that their symmetric difference has arbitrarily small capacity (Caffarelli and Lin 2007). Formally speaking, these are a class of general sets which can be used to define a weak form of elliptic equations. For example, all open sets are quasi-open. The set  $\mathcal{A}(\Omega)$  of quasi-open sets in a domain  $\Omega$  can be equipped with a notion of weak convergence by defining that a sequence of quasi-open sets  $\{A_n\}$  weakly converges to  $A \in \mathcal{A}(\Omega)$  if  $\eta_{A_n} \rightarrow \eta_A$  weakly in  $H^1(\Omega)$  and  $A = \{\eta_A > 0\}$  where  $\eta_\omega \in H^1(\Omega)$  is the extension to  $\Omega$  by zero of the unique weak solution of

$$-\Delta \eta_\omega = 1 \quad \text{in } \omega \quad \text{and} \quad \eta_\omega = 0 \quad \text{on } \partial\omega.$$

Using these notions it is possible to establish that the spectral functional is lower semi-continuous with respect to weak convergence in  $\mathcal{A}(\Omega)$  and existence of an  $m$ -partition into quasi-open sets follows from the direct method of the calculus of variations (Caffarelli and Lin 2007).

An alternative method is based on using the eigenfunctions to partition the domain using a approach formulated by Caffarelli and Lin (2007). The energy (1.1) is transformed into a functional form as a constrained Dirichlet energy:

**Problem 1.2.** Given a positive integer  $m$  and a smooth surface  $\Gamma$ , find  $\mathbf{u} = (u_1, \dots, u_m) \in H^1(\Gamma, \Xi)$  with  $\|u_i\|_{L^2(\Gamma)} = 1$  for  $i = 1, \dots, m$ , to minimise

$$\mathcal{E}_{\text{SEG}}^0(\mathbf{u}) = \sum_{i=1}^m \int_{\Gamma} |\nabla_{\Gamma} u_i|^2 \, d\sigma, \quad (1.2)$$

where  $\Xi \subset \mathbb{R}^m$  is the singular set

$$\Xi = \left\{ \mathbf{y} = (y_1, \dots, y_m) \in \mathbb{R}^m : \sum_{i=1}^m \sum_{i \neq j} y_i^2 y_j^2, y_k \geq 0 \, k = 1, 2, \dots, m \right\}.$$

It was shown by Caffarelli and Lin (2007) that (1.2) is equivalent to (1.1) when we restrict to  $m$ -partitions of  $\Gamma$  in which  $\Gamma_i$  are quasi-open sets. Let  $\{\Gamma_i\}_{i=1}^m$  be a minimiser of (1.1) consisting of quasi-open sets, then if  $u_i$  is the first eigenfunction of the Dirichlet Laplace–Beltrami operator over  $\Gamma_i$ , for  $i = 1, \dots, m$ , the vector quantity  $\mathbf{u} = (u_1, \dots, u_m)$  is a minimiser of (1.2). Conversely, let the function  $\mathbf{u} = (u_1, \dots, u_m) \in H^1(\Gamma, \Xi)$  be a minimiser of (1.2), then setting  $\Gamma_i = \{u_i > 0\}$ , for

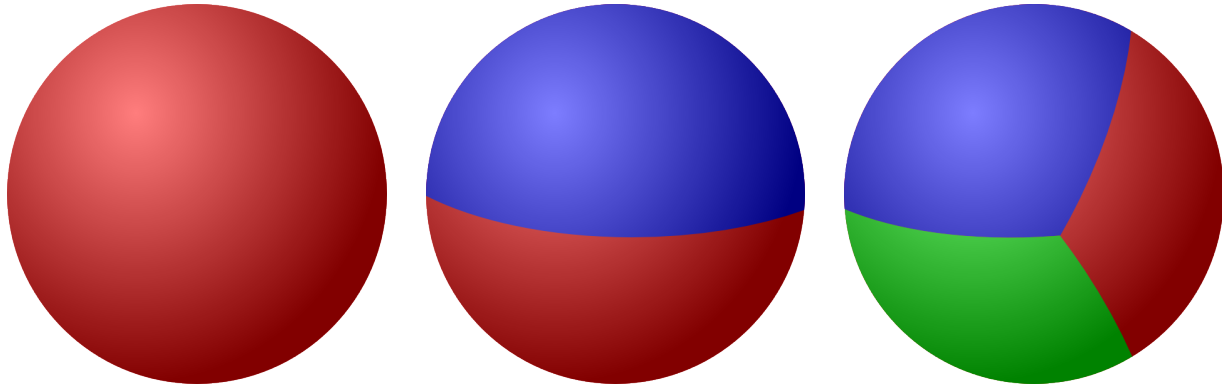


Figure 1: Plots of the known cases when  $\Gamma$  is a sphere,  $m = 1$  (left),  $m = 2$  (center) and  $m = 3$  (right) (Helfffer et al. 2010).

$i = 1, \dots, m$ , the collection of quasi-open sets  $\{\Gamma_i\}_{i=1}^m$  is an  $m$ -partition of  $\Gamma$  which is a minimiser of (1.1) and

$$\lambda_1(\Gamma_i) = \int_{\Gamma} |\nabla_{\Gamma} u_i|^2 \, d\sigma \quad \text{for } i = 1, \dots, m.$$

The authors Caffarelli and Lin (2007) use this formulation to show existence of minimisers and regularity of the interface between partitions.

Other works by Conti, Terracini and Verzini (2002, 2003) and Caffarelli and Lin (2007, 2008) have focused on regularity and more qualitative aspects of the problem for a Cartesian domain. Conti, Terracini and Verzini derive optimality conditions, such as the gradient of eigenfunctions should match at partition boundaries, and also that the partition consists of open sets. Caffarelli and Lin obtain regularity results, such as  $C^{1,\alpha}$ -smoothness of the partition boundaries away from a set of codimension two, and also an estimate of the behaviour in the limit of large  $m$ . In particular, they prove that the optimal energy is bounded above and below by a constant times the  $m$ th eigenvalue on  $\Gamma$  and conjecture that for large  $m$  the optimal partition will be asymptotically close to a hexagonal tiling in the case of a planar domain. The problem can be seen as a the strong competition limit of segregating species either in Bose-Einstein condensate (Chang, Lin, Lin and Lin 2004), population dynamics (Conti, Terracini and Verzini 2005a,b) and materials science (Chen 2002) in curved geometries.

The curved hypersurface problem has been studied analytically in the case that  $\Gamma$  is a sphere in recent work of Helfffer, Hoffmann-Ostenhof and Terracini (2010). They show the optimal partition is given by two hemispheres for the case  $m = 2$  and the so-called Y-partition for  $m = 3$ ; see Figure 1 and section 3.1. Furthermore, they show that for each  $m$  there is an optimal partition which satisfies an equal angle condition which says that the boundary arcs that meet at a critical point do so with equal angles.

Numerical studies of this type of problem have so far been limited to the planar case. We mention in particular the studies of Chang et al. (2004) and Bonnaillie-Noël, Helfffer and Vial (2010) and some special algorithms in the case of small  $m$  given by Bozorgnia and Arakelyan (2013) and

Bozorgnia (2009). Also Bourdin, Bucur and Oudet (2010) considered the problem for large values of  $m$  using a fictitious domain approach. This problem has also been considered on graphs (Coifman and Lafon 2006; Osting, White and Oudet 2014) with applications in big data segmentation. Finally, we mention the study which will be the basis of our work in the paper: an eigenfunction segregation approach (Du and Lin 2009). We will describe the algorithm in more detail in the following.

We derive computational approaches using the surface finite element method (Dziuk 1988; Dziuk and Elliott 2007) to find solutions to these problems. A review of computational techniques for partial differential equations on surfaces is given by Dziuk and Elliott (2013). Our methods will be one of the algorithms given by Du and Lin (2009) applied with the surface finite element method in order to explore Problem 1.1.

We believe some of the techniques used in this paper, such as operator splitting and parallel computing, could be applied in a wide range of multiphase problems; for example Gräser, Kornhuber and Sack (2014). In these problems, one typically has a large system of reaction diffusion systems to solve with small parameter  $\varepsilon$  indicating an interfacial width. The small parameter  $\varepsilon$  acts with nonlinear terms to separate different phases. Our methods are designed to be transferable to this type of problem also. In contrast to many multiphase problems, the dynamic problem considered in this paper are based on non-local interface motion.

## 1.1 Approximation approach

One could try to directly compute the gradient flow of the energy  $\mathcal{E}_{\text{SEG}}^0$  in (1.2); see Mayer (1998) for analytic considerations of this approach. However, this would lead to equations which would be hard to discretise. We instead relax the constraint that  $\mathbf{u}$  takes values in  $\Xi$  by adding a penalty term to the energy functional following Caffarelli and Lin (2008). In this way, we consider the extended energy functional:

$$\mathcal{E}_{\text{SEG}}^\varepsilon(\mathbf{u}^\varepsilon) = \sum_{i=1}^m \frac{1}{2} \int_{\Gamma} |\nabla u_i^\varepsilon|^2 \, d\sigma + \int_{\Gamma} F_\varepsilon(\mathbf{u}^\varepsilon) \, d\sigma, \quad F_\varepsilon(\mathbf{u}^\varepsilon) = \frac{1}{\varepsilon^2} \sum_{i=1}^m \sum_{\substack{j=1 \\ j \neq i}}^m (u_i^\varepsilon)^2 (u_j^\varepsilon)^2.$$

**Problem 1.3.** Given a positive integer  $m$ , a smooth surface  $\Gamma$  and  $\varepsilon > 0$ , find  $\mathbf{u}^\varepsilon = (u_1^\varepsilon, \dots, u_m^\varepsilon) \in H^1(\Gamma, \mathbb{R}^m)$  with  $\|u_i^\varepsilon\|_{L^2(\Gamma)} = 1$  for  $i = 1, \dots, m$ , to minimise

$$\mathcal{E}_{\text{SEG}}^\varepsilon(\mathbf{u}^\varepsilon) = \sum_{i=1}^m \frac{1}{2} \int_{\Gamma} |\nabla u_i^\varepsilon|^2 \, d\sigma + \int_{\Gamma} F_\varepsilon(\mathbf{u}^\varepsilon) \, d\sigma. \quad (1.3)$$

We will now compute the gradient flow of this relaxed problem. We now seek a time dependent function  $\mathbf{u}^\varepsilon: \Gamma \times \mathbb{R}_+ \rightarrow \mathbb{R}^m$  and  $\lambda^\varepsilon: \mathbb{R}_+ \rightarrow \mathbb{R}^m$  satisfying

$$\partial_t u_i^\varepsilon = \Delta_{\Gamma} u_i^\varepsilon + \lambda_i u_i^\varepsilon - \frac{2}{\varepsilon^2} \left( \sum_{j \neq i} (u_j^\varepsilon)^2 \right) u_i^\varepsilon \quad \text{on } \Gamma \times \mathbb{R}_+, \text{ for } i = 1, \dots, m, \quad (1.4a)$$

$$\mathbf{u}^\varepsilon(\cdot, 0) = \mathbf{u}^0 \quad \text{on } \Gamma, \quad (1.4b)$$

subject to the constraint

$$\int_{\Gamma} |u_i^\varepsilon|^2 \, d\sigma = 1 \quad \text{for } i = 1, \dots, m. \quad (1.5)$$

Here, we suppose that the initial condition partitions  $\Gamma$  and has unit norm:

$$\mathbf{u}^0 \in H^1(\Gamma, \Xi), \quad \int_{\Gamma} |u_i^0|^2 \, d\sigma = 1 \quad \text{for } i = 1, \dots, m.$$

We remark that  $u_i^0 \geq 0$  implies  $u_i^\varepsilon \geq 0$  for  $i = 1, \dots, m$ .

This gradient flow problem was studied by Caffarelli and Lin (2009) for Cartesian geometries. The proofs can be easily transferred onto surfaces. We recall their results stated on surfaces:

$$\lambda_i^\varepsilon(t) = \int_{\Gamma} |\nabla u_i^\varepsilon|^2 + \frac{2}{\varepsilon^2} \left( \sum_{j \neq i} (u_j^\varepsilon)^2 \right) (u_i^\varepsilon)^2 \, d\sigma,$$

and

$$\mathcal{E}_{\text{SEG}}^\varepsilon(\mathbf{u}^\varepsilon) \leq \sum_{i=1}^m \lambda_i^\varepsilon(t) = \mathcal{E}_{\text{SEG}}^\varepsilon(\mathbf{u}^\varepsilon) + 2 \int_{\Gamma} F_\varepsilon(\mathbf{u}^\varepsilon) \, d\sigma.$$

Furthermore, they show that  $\mathcal{E}_{\text{SEG}}^\varepsilon(\mathbf{u}^\varepsilon)$  is a monotone decreasing function of time for  $\mathbf{u}^\varepsilon$  the solution of (1.4). This implies the existence of a unique global strong solution  $\mathbf{u}^\varepsilon \in L^\infty(\mathbb{R}_+, H^1(\Gamma, \mathbb{R}^m))$  for each  $\varepsilon > 0$ . Finally, they give estimates of interest when considering the sharp interface limit: Denoting by  $\bar{\mathbf{u}}^\varepsilon$  the minimiser of the  $\varepsilon$ -problem, for any  $0 < t_1 < t_2$ , we have

$$\int_{t_1}^{t_2} \int_{\Gamma} F_\varepsilon(\bar{\mathbf{u}}^\varepsilon) \, d\sigma \, dt \rightarrow 0 \quad \text{as } \varepsilon \rightarrow 0,$$

and that the limit of minimising functions as  $\varepsilon \rightarrow 0$ ,  $\bar{\mathbf{u}}^\varepsilon$  converges strongly in  $H^1(\Gamma \times \mathbb{R}_+)$  to a suitable weak solution of the constrained gradient flow of (1.2).

A key advantage of this approach is that we are trying to approximate smooth functions  $\mathbf{u}^\varepsilon$  in place of the domains  $\Gamma_i$ . The limiting function  $\mathbf{u}^* = (u_1^*, \dots, u_m^*)$ , is the limit of  $\mathbf{u}^\varepsilon$  as  $\varepsilon \rightarrow 0$  partitions  $\Gamma$  so we can define  $\Gamma_i = \{u_i^* > 0\}$  and  $u_j^* = 0$  in  $\Gamma_j$ ,  $j \neq i$ . We note also that setting  $v_i^* := u_i^* - \sum_{j \neq i} u_j^*$  we have  $\Gamma_i = \{v_i^* > 0\}$ . A possible disadvantage of this method is that it is not clear how to relate  $\mathbf{u}^\varepsilon$  to a partition  $\{\Gamma_i\}$  when  $\varepsilon$  is fixed. Possibilities for defining  $\Gamma_i^\varepsilon$  include  $\Gamma_i^\varepsilon = \{u_i^\varepsilon > c(\varepsilon)\}$  or  $\Gamma_i^\varepsilon = \{v_i^\varepsilon > 0\}$  where  $v_i^\varepsilon := u_i^\varepsilon - \sum_{j \neq i} u_j^\varepsilon$ .

## 1.2 Outline

In the remainder of this paper, we will give a suitable discretisation of this approach using the surface finite element method. We will propose an algorithm to solve the discretised optimisation problem and give practical details of how we implement this method. Our experience is that the eigenfunction segregation method performs very well. Our results section consists of three parts. First, we will test our algorithm in the case of three partitions on the sphere for which we know the absolute minimiser. We will then compute partitions of the sphere for larger values of  $m$  and make some observations about the structure. Finally we consider other surfaces to see the different effects of curvature and different genus surfaces. The computations lead to some natural conjectures.

## 2 Computational method

### 2.1 Discretisation

We start the discretisation by taking a polyhedral approximation  $\Gamma_h$  of  $\Gamma$ . We assume that  $\Gamma_h$  consists of a shape regular triangulation  $\mathcal{T}_h$  where  $h$  is the maximal diameter of a simplex (triangle for  $n = 2$ ) in  $\mathcal{T}_h$ . We will denote by  $\mathcal{N}_h$  the vertices of  $\Gamma_h$  and call  $\Gamma_h$  a triangulated surface. We suppose that  $\Gamma_h$  interpolates  $\Gamma$  in the sense that the vertices of triangles of  $\Gamma_h$  lie on  $\Gamma$ .

Over this triangulation, we define two continuous finite element spaces, a space of scalar valued functions  $S_h$  and a space of vector valued functions  $\mathbf{S}_h$ . These are given by

$$\begin{aligned} S_h &= \{\chi_h \in C(\Gamma_h) : \chi_h|_T \text{ is affine linear, for all } T \in \mathcal{T}_h\} \\ \mathbf{S}_h &= \{\boldsymbol{\eta}^h = (\eta_1^h, \dots, \eta_m^h) \in C(\Gamma_h; \mathbb{R}^m) : \eta_i^h \in S_h \text{ for } i = 1, \dots, m\}. \end{aligned}$$

We can directly formulate the discrete version of Problem 1.3.

**Problem 2.1.** Given a positive integer  $m$ , a triangulated surface  $\Gamma_h$  and  $\varepsilon > 0$ , find  $\mathbf{u}^{\varepsilon, h} = (u_1^{\varepsilon, h}, \dots, u_m^{\varepsilon, h}) \in \mathbf{S}_h$  to minimise

$$\mathcal{E}_{\text{SEG}}^{\varepsilon, h}(\mathbf{u}^{\varepsilon, h}) = \sum_{i=1}^m \int_{\Gamma_h} |\nabla_{\Gamma_h} u_i^{\varepsilon, h}|^2 d\sigma_h + \int_{\Gamma_h} F_\varepsilon(\mathbf{u}^{\varepsilon, h}) d\sigma_h. \quad (2.1)$$

Our optimisation strategy will be to directly solve a discretisation of the gradient flow equations. Discretising in space first, we seek a time dependent finite element function  $\mathbf{u}^{\varepsilon, h} \in C^1(\mathbb{R}_+; \mathbf{S}_h)$  and  $\lambda^{\varepsilon, h} : \mathbb{R}_+ \rightarrow \mathbb{R}^m$  satisfying  $\|u_i^{\varepsilon, h}\|_{\Gamma_h}^2 = 1 \quad i = 1, 2, \dots, m$ ,

$$\begin{aligned} & \int_{\Gamma_h} \partial_t u_i^{\varepsilon, h} \chi_h + \nabla_{\Gamma_h} u_i^{\varepsilon, h} \cdot \nabla_{\Gamma_h} \chi_h d\sigma_h \\ &= \int_{\Gamma_h} \lambda_i^{\varepsilon, h} u_i^{\varepsilon, h} \chi_h - \frac{2}{\varepsilon^2} \left( \sum_{j \neq i} (u_j^{\varepsilon, h})^2 \right) u_i^{\varepsilon, h} \chi_h d\sigma_h \quad \text{for all } \chi_h \in S_h \\ & \mathbf{u}^{\varepsilon, h}(\cdot, 0) = \mathbf{u}^{h, 0}. \end{aligned} \quad (2.2)$$

Here,  $\mathbf{u}^{h, 0} = (u_1^{h, 0}, \dots, u_m^{h, 0})$  is initial data in  $\mathbf{S}_h$  such that  $(u_i^{h, 0})^2 (u_j^{h, 0})^2 = 0$  for all  $i, j = 1, \dots, m$  with  $i \neq j$ .

We discretise in time using a operator splitting strategy similar to a scheme proposed by Du and Lin (2009). At each time step, we first solve one step of the heat equation, then solve an ordinary differential equation for the nonlinear terms, and use a projection to deal with the Lagrange multiplier.

### 2.2 Computational method

The operator splitting method is as follows.

**Algorithm 2.2.** Given  $\varepsilon > 0$ , a positive integer  $m$ , a time step  $\tau > 0$  and an initial condition  $\mathbf{u}_0^h = ((u_1^h)_0, \dots, (u_m^h)_0) \in \mathcal{S}_h$  with  $(u_i^h)_0(z)(u_j^h)_0(z)^2 = 0$  for all  $z \in \mathcal{N}_h$  and  $i, j = 1, \dots, m$  with  $i \neq j$ , for  $k = 0, 1, 2, \dots$ ,

1. Solve one time step of the heat equation for  $i = 1, \dots, m$  using implicit Euler. We wish to find  $\tilde{\mathbf{u}}^{\varepsilon, h} = (\tilde{u}_1^{\varepsilon, h}, \dots, \tilde{u}_m^{\varepsilon, h}) \in \mathcal{S}_h$

$$\int_{\Gamma_h} \frac{1}{\tau} (\tilde{u}_i^{\varepsilon, h} - (u_i^{\varepsilon, h})_k) \chi_h + \nabla_{\Gamma_h} \tilde{u}_i^{\varepsilon, h} \cdot \nabla_{\Gamma_h} \chi_h \, d\sigma_h = 0 \quad \text{for all } \chi_h \in S_h, i = 1, \dots, m.$$

2. Solve the nonlinear terms exactly as ordinary differential equation at each node. For all nodes  $z \in \mathcal{N}_h$  and  $i = 1, \dots, m$ , find  $\hat{u}_i^{\varepsilon, h}(z): [t^k, t^{k+1}] \rightarrow \mathbb{R}$  such that

$$\frac{d}{dt} \left( \hat{u}_i^{\varepsilon, h}(z)(t) \right) = - \left( \frac{1}{\varepsilon^2} \sum_{j \neq i} (\tilde{u}_j^{\varepsilon, h}(z))^2 \right) \hat{u}_i^{\varepsilon, h}(z)(t), \quad \hat{u}_i^{\varepsilon, h}(z)(t^k) = \tilde{u}_i^{\varepsilon, h}(z).$$

3. Find the new solution  $(\mathbf{u}^{\varepsilon, h})_{k+1}$  by normalising the final time solution  $(\hat{u}_1^{\varepsilon, h}(\cdot)(t^{k+1}), \dots, \hat{u}_m^{\varepsilon, h}(\cdot)(t^{k+1}))$ :

$$(u_i^{\varepsilon, h}(z))_{k+1} = \frac{\hat{u}_i^{\varepsilon, h}(z)(t^{k+1})}{\left\| \hat{u}_i^{\varepsilon, h}(\cdot)(t^{k+1}) \right\|_{L^2(\Gamma_h)}} \quad \text{for all } z \in \mathcal{N}_h, i = 1, \dots, m.$$

Similarly to [Bao and Du \(2004\)](#), one can show an energy decreasing property for this scheme. The method is the same as the scheme of [Du and Lin \(2009\)](#) except we exchange a Gauss-Seidel iteration in step 2 for a Jacobi iteration. The ordinary differential equation from step 2 can be solved exactly to give:

$$\hat{u}_i^{\varepsilon, h}(z)(t^{k+1}) = \tilde{u}_i^{\varepsilon, h}(z) \exp \left( - \frac{\tau}{\varepsilon^2} \sum_{j \neq i} (\tilde{u}_j^{\varepsilon, h}(z)(t))^2 \right).$$

Using this solution, we write a more practical version of step 2 as

2. For each node  $z \in \mathcal{N}_h$ ,
  - (a) For  $i = 1, \dots, m$ , compute  $\tilde{u}_i^{\varepsilon, h}(z)^2$ ;
  - (b) Find  $S = \sum_{i=1}^m \tilde{u}_i^{\varepsilon, h}(z)^2$ ;
  - (c) For  $i = 1, \dots, m$ , compute  $\hat{u}_i^{\varepsilon, h}(z)(t^{k+1})$  by

$$\hat{u}_i^{\varepsilon, h}(z)(t^{k+1}) = \tilde{u}_i^{\varepsilon, h}(z) \exp \left( - \frac{\tau}{\varepsilon^2} (S - \tilde{u}_i^{\varepsilon, h}(z)^2) \right)$$

We stop the computation when the change in energy is less than  $10^{-6}$ . In order to reduce the computational cost this is only calculated every  $M_\tau$  iterations where  $0.1 = M_\tau \tau$ .

Since, in general, we do not know the configuration of the optimal domains, we initialise the computations with a random initial condition. We loop over the grid nodes  $z \in \mathcal{N}_h$  and uniformly at random choose one value  $i \in \{1, \dots, m\}$  and set  $(u_0^h)(z)_i = 1$  and  $(u_0^h)(z)_j = 0$  for  $j \neq i$  then normalise each component,  $(u_0^h)_i$ , for  $i = 1, \dots, m$ , in  $L^2(\Gamma)$ . As a result the first linear solve for the heat equation step will take more iterations, however the difference is not significant in this case.

**Remark.** In practice, we find this operator splitting method to be stable and efficient. If we discretised (2.2) in time directly using the Lagrange multiplier, we would have the choice to take the Lagrange multiplier implicitly or explicitly. An implicit discretisation would leave a fully coupled system of equations to solve, which would not be so easily implemented using parallel high performance computing techniques. An explicit discretisation would imply a time step restriction based on the size of the maximum  $H^1$ -semi norm of each component. We wish to start with a random initial condition in order to avoid local minima, however this has a very large  $H^1$ -semi norm which would give an unfeasible time step restriction. All three methods are considered for the flat problem in the time discrete-space continuous case by [Du and Lin \(2009\)](#).

## 2.3 Parallel computations

The algorithm has been formulated so that we can use high performance computing to implement the optimisation. The key idea is to store the solution over  $m$  parallel processors and perform most of the computations on a single processor. Communication between processors is kept to a minimum.

We distribute the solution  $\mathbf{u}^{\varepsilon,h}$  over  $m$  processors so that processor  $i$  stores  $u_i^{\varepsilon,h}$ . At each time step, each processor performs one linear solve (step 1), one loop over all nodes communicating with all other nodes to perform the sum in step 2(b) (step 2), then one more loop over all nodes to normalise the solution (step 3). In particular, computing sum in step 2(b) over all  $j$  is more efficient than computing the sum over all other  $j \neq i$ .

A similar approach was also taken to parallelisation by [Bourdin et al. \(2010\)](#) who computed up to 512 partitions. Our approach performs very well for  $m \leq 32$ . At the moment we restricted to this number of partitions because we wish to have a meaningful number of elements in each partition. It is possible that one may gain efficiency by using an adaptive mesh refinement on the unstructured grids enabling sufficiently accurate computations with a larger number of partitions. This is left for future work.

All test cases were implemented using the Distributed and Unified Numerics Environment (DUNE) ([Bastian, Blatt, Dedner, Engwer, Klöforn, Ohlberger and Sander 2008b](#); [Bastian, Blatt, Dedner, Engwer, Klöforn, Kornhuber, Ohlberger and Sander 2008a](#)). Matrices are assembled using the DUNE-FEM ([Dedner, Klöforn, Nolte and Ohlberger 2010](#)) and solved using a conjugate gradient method preconditioned with algebraic multigrid Jacobi preconditioner from DUNE-ISTL ([Blatt and Bastian 2007](#)). Parallelisation is performed using MPI. All visualisation is performed in ParaView ([Henderson 2014](#)). The code we have written for the simulations in this paper is available at



### 3 Results

#### 3.1 Convergence tests for three partitions of the sphere

From the work of Helffer et al. (2010), we know that the Y-partition is optimal in the case  $m = 3$  on the sphere. This corresponds (up to rotations of the sphere) to  $\Gamma_1 = \{0 < \varphi < 2\pi/3\}$ ,  $\Gamma_2 = \{-2\pi/3 < \varphi < 0\}$  and  $\Gamma_3 = \{|\varphi| > 2\pi/3\}$ . We can compute that the first eigenfunctions are:

$$\begin{aligned} u_1(\theta, \varphi) &= \sin\left(\frac{3\phi}{2}\right)(\sin \theta)^{\frac{3}{2}} && \text{on } \Gamma_1 \\ u_2(\theta, \varphi) &= -\sin\left(\frac{3\phi}{2}\right)(\sin \theta)^{\frac{3}{2}} && \text{on } \Gamma_2 \\ u_3(\theta, \varphi) &= \sin\left(\frac{3|\phi|}{2} - \pi\right)(\sin \theta)^{\frac{3}{2}} && \text{on } \Gamma_3. \end{aligned}$$

Each of these eigenfunctions has eigenvalue  $15/4$ .

We first test convergence with respect to the discretisation parameters. We perform our algorithm at  $\varepsilon = 5 \cdot 10^{-3}$  and  $\tau = 10^{-4}$  over five levels of mesh refinement, reducing from  $h = 3.21614 \cdot 10^{-2}$  to  $h = 2.01073 \cdot 10^{-3}$ . We compute until  $t = 2$ . We have plotted the energy along the time evolution in Figure 2 and see good convergence. We have also included a dashed line at the exact energy  $45/4$  for  $\varepsilon = 0$ . We see that for a given  $\varepsilon$  the error in energy can be large.

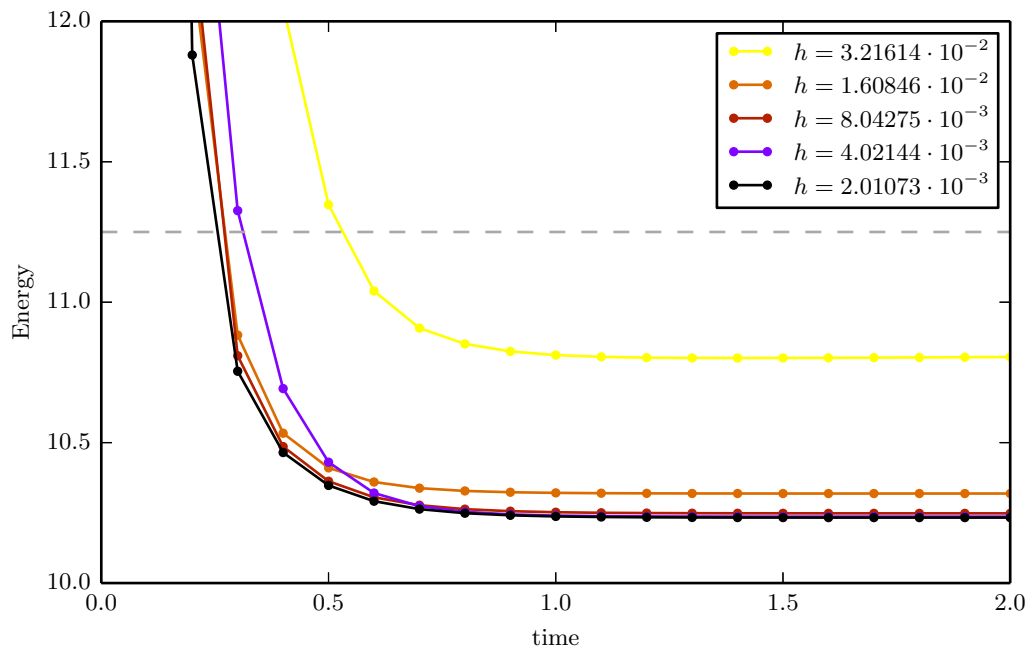


Figure 2: Convergence with respect to discretisation parameters for  $\varepsilon = 5 \cdot 10^{-3}$  to the Y-partition on the sphere. The dashed grey line is the exact energy for  $\varepsilon = 0$ .

To test the convergence of the regularisation we compute the minimizer for a sequence for values for  $\varepsilon$ . We start on a coarse mesh with  $\tau = 8 \cdot 10^{-4}$ , once we have reached a minimizer, we refine



$\varepsilon$	Energy	Energy error	(eoc)	$S_\varepsilon$	(eoc)
$5.00000 \cdot 10^{-1}$	1.9100	9.3400	—	1.9098	—
$2.50000 \cdot 10^{-1}$	4.8759	6.3741	0.5512	1.5350	0.3151
$1.25000 \cdot 10^{-1}$	6.6257	4.6243	0.4630	1.0548	0.5413
$6.25000 \cdot 10^{-2}$	7.8829	3.3671	0.4577	0.7751	0.4444
$3.12500 \cdot 10^{-2}$	8.8095	2.4405	0.4643	0.5714	0.4400
$1.56250 \cdot 10^{-2}$	9.4907	1.7593	0.4721	0.4188	0.4482
$7.81250 \cdot 10^{-3}$	9.9880	1.2620	0.4793	0.3050	0.4576
$3.90625 \cdot 10^{-3}$	10.3487	0.9013	0.4856	0.2209	0.4652
$1.95312 \cdot 10^{-3}$	10.6088	0.6412	0.4912	0.1605	0.4605
$9.76562 \cdot 10^{-4}$	10.7958	0.4542	0.4974	0.1168	0.4591

Table 1: Results of convergence test in  $\varepsilon$  for numerical tests for three partition case. Energy is  $\mathcal{E}_{\text{SEG}}^\varepsilon$  at the best computed partition, energy error is the difference to  $45/4$  the exact energy for  $\varepsilon = 0$ , and  $S_\varepsilon$  is given by (3.1).

the mesh by bisecting elements once (two bisections reduces  $h$  roughly by half) and reduce  $\tau$  by a factor  $1/\sqrt{2}$ . Instead of computing a new random initial condition after each refinement, we use the previous minimiser as the new initial condition.

We define  $S_\varepsilon$  to be part of the energy associated with regularisation:

$$S_\varepsilon(\mathbf{u}^{\varepsilon,h}) := \int_{\Gamma_h} F_\varepsilon(\mathbf{u}^{\varepsilon,h}) d\sigma_h = \frac{1}{\varepsilon^2} \int_{\Gamma_h} \sum_{i=1}^m \sum_{j \neq i} (u_i^{\varepsilon,h})^2 (u_j^{\varepsilon,h})^2 d\sigma_h. \quad (3.1)$$

These values illustrate the convergence of the relaxation to the exact problem. We expect  $S_\varepsilon \rightarrow 0$  as we know that we recover the a minimiser of the partition problem as  $\varepsilon \rightarrow 0$ .

We have computed the full and regularisation energy at each minimiser. The results are shown in Table 1 and Figure 3. The tables also show the experimental order of convergence (eoc) which is computed via the formula

$$(\text{eoc})_i = \frac{\log(\text{error}_i/\text{error}_{i-1})}{\log(1/2)}.$$

where  $\text{error}_i$  is the error in energy against the exact partition at refinement level  $i$ .

The eigenfunction segregation approach performs very well with respect to convergence in  $\varepsilon$ . We observe order  $\varepsilon^{\frac{1}{2}}$  convergence both for the full energy and also for  $S_\varepsilon$ . The errors are still quite large for reasonable sized values of  $\varepsilon$  so we must take very small values of  $\varepsilon$  to trust any predictions of energy values using this method.

### 3.2 Computed partitions of the sphere for $m \geq 3$

We proceed with the following refinement rules. We initialise the problem with a random initial condition for  $\varepsilon_0 = \frac{1}{2}$ ,  $\tau_0 = 8 \cdot 10^{-4}$  on a mesh  $\Gamma_{h,0}$ , then for  $l = 0, 1, 2, \dots$ , we find a minimiser of the  $\varepsilon_l$ -problem on  $\Gamma_{h,l}$ , then refine the mesh globally by bisecting all elements, and find  $\varepsilon_{l+1}$  and

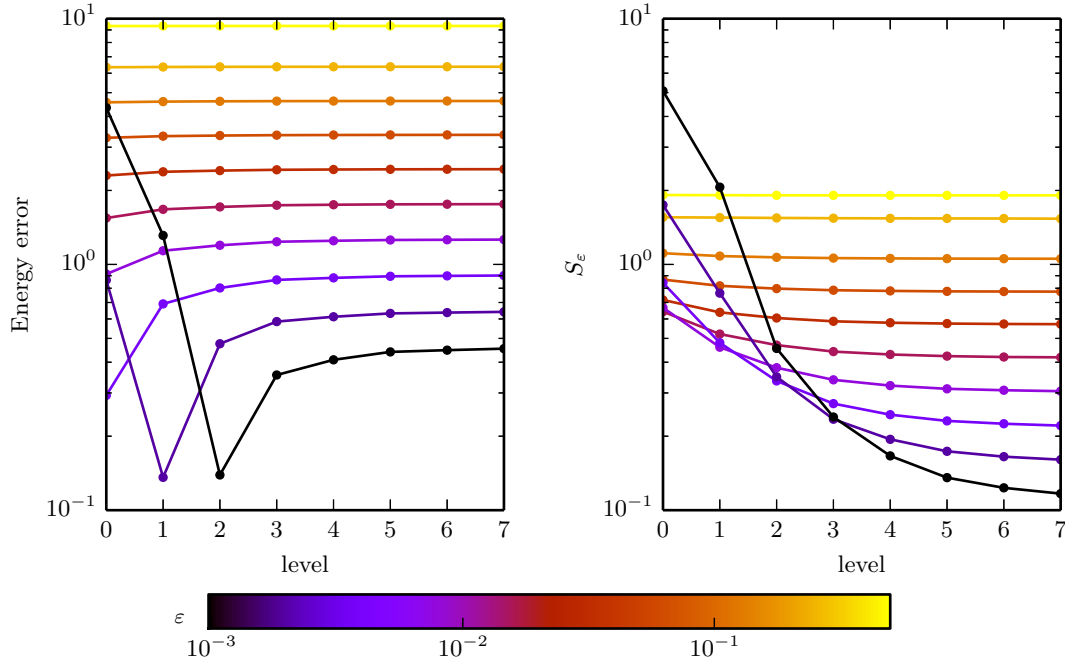


Figure 3: Convergence with respect to  $\varepsilon$  to the Y-partition on the sphere. The energy error is difference to  $45/4$  the exact energy for  $\varepsilon = 0$ , and  $S_\varepsilon$  is given by (3.1).

$\tau_{l+1}$  as

$$\varepsilon_{l+1} = \sqrt{2}\varepsilon_l \quad \tau_{l+1} = \sqrt{2}\tau_l.$$

We use the optimal function for level  $l - 1$  as the initial condition on level  $l$ . The final parameters are given in Table 2.

Plots of the solutions for several values of  $m$  are given in Figures 4. Observe that the colour coding of these figures indicates the partitions using the computed values of the eigenfunctions. Eigenvalue estimates are computing by taking the mean  $H^1$ -semi norm of the components. The computed eigenvalues are plotted in Figure 5. Theorem 3 of the work by Caffarelli and Lin (2007) proves that the energy scales like  $\lambda_m(\Gamma)$  up to a constant factor. Using Weyl’s asymptotics, we see

$m$	$l$	Degrees of freedom	$\varepsilon$
3	9	579 830	$6.25 \cdot 10^{-4}$
4	9	786 440	$6.25 \cdot 10^{-4}$
5	9	983 050	$6.25 \cdot 10^{-4}$
6	9	1 179 660	$6.25 \cdot 10^{-4}$
7	9	1 376 270	$6.25 \cdot 10^{-4}$
8	7	196 624	$1.25 \cdot 10^{-3}$
16	7	393 248	$1.25 \cdot 10^{-3}$
32	7	786 496	$1.25 \cdot 10^{-3}$

Table 2: Final parameters for computations on the sphere.

that in two space dimensions this means that the average eigenvalue is bounded above and below by  $m$  times a constant. This is indicated by the blue line which is  $m$  times the first eigenvalue corresponding to a hexagon  $H$  of area  $4\pi$  (the surface area of the sphere) – this is the conjectured average eigenvalue for large  $m$  in the plane (Caffarelli and Lin 2007). Our results indicate a similar scaling property for the sphere.

Rather than just using the computed eigenfunction values, as mentioned earlier, we may define an approximate partition by

$$\Gamma_i^{\varepsilon,h} := \left\{ x \in \Gamma : v_i^{\varepsilon,h}(x) := u_i^{\varepsilon,h}(x) - \sum_{j \neq i} u_j^{\varepsilon,h}(x) > 0 \right\} \quad \text{for } i = 1, \dots, m. \quad (3.2)$$

We motivate the use of this definition by noting that each  $u_i^{\varepsilon,h}$  is positive and the supports of  $\{u_i^{\varepsilon,h}\}$  overlap, hence this function is zero only surrounding one partition where  $u_i^{\varepsilon,h} = u_j^{\varepsilon,h}$  for some  $j \neq i$ . Note that these sets will not cover  $\Gamma$  and there will be a small void between regions. Furthermore we may use  $v_i^{\varepsilon,h}$  in the following interesting way. Suppose that  $\gamma$  is a curve on  $\Gamma$  defined by as the zero level set of a function  $\phi$ ,  $\gamma = \{\phi = 0\}$ , then the geodesic curvature of  $\gamma$ , which we denote by  $\kappa_g$  is given by

$$\kappa_g = \nabla_{\Gamma} \cdot \left( \frac{\nabla_{\Gamma} \phi}{|\nabla_{\Gamma} \phi|} \right). \quad (3.3)$$

We can use ParaView’s gradient reconstruction function to compute an approximation of  $\kappa_g$  over the interface at the boundary of each partition  $\Gamma_i$  using  $\phi = v_i^{\varepsilon,h}$ . An example of this is shown in Figure 6. We see that this value is small away from junctions.

We observe that at junctions three partitions coincide with equal angles. See, for example, Figure 7. This is consistent with the results of Helffer et al. (2010) who prove that all partitions have an equal angle property. From our results it is difficult to quantify this result since at any triple point there is a void region because of our regularisation. Also in Figure 7, we have superimposed an equal angle triple junction which shows good agreement to results we have. We can consider a reduced problem of finding the first eigenvalue over partitions of the unit disk. We find with three equal partitions (similar to the Y-partition) the total energy is approximately  $60.6 (= 3 \cdot 20.2)$  and for four partitions, one in each quadrant, the total energy is approximately  $105.6 (= 4 \cdot 26.4)$ . Taking three partitions leads to a significant reduction in energy.

Table 3 shows one representative of each polygon similarity class and more details of the best estimate of the energy and also the similarity classes of polygons. The energy calculation shows the values of each eigenvalue (mean and standard deviation for each similarity class of polygons) and also  $S_{\varepsilon}$  for each of the final configurations.

There are several striking features:

- All partitions consist of curvi-linear polygons;
- The boundary of each partition consists of arcs with zero geodesic curvature (“straight lines”);

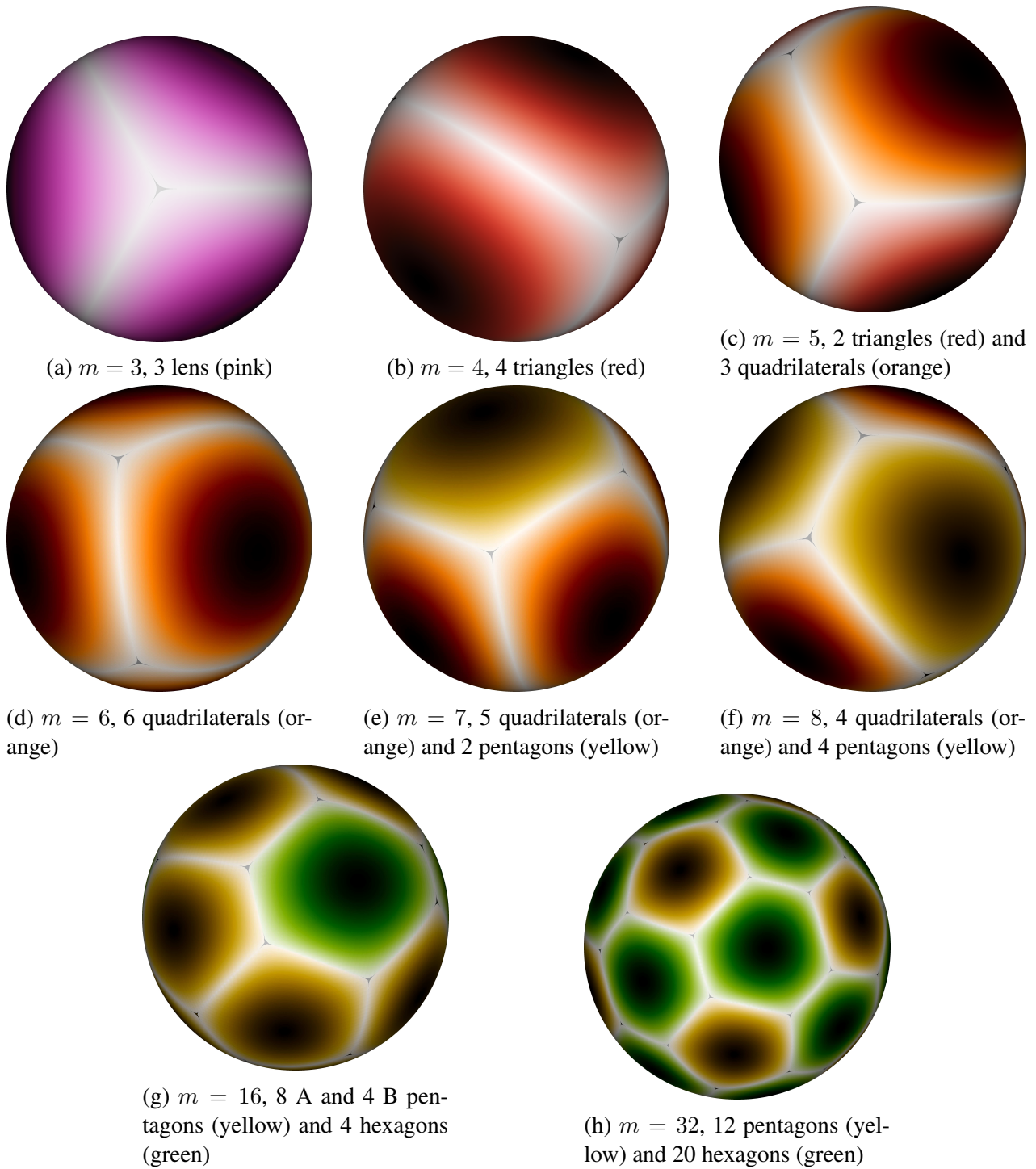


Figure 4: Plots of the minimising configurations  $\{\Gamma_i^{\varepsilon, h}\}_{i=1}^m$  with void regions in grey. Colours only in the online version. Each partition is coloured according to the polygon type and shaded by the eigenfunction from white for  $u_i = 0$  to black for  $u_i$  at the maximum.

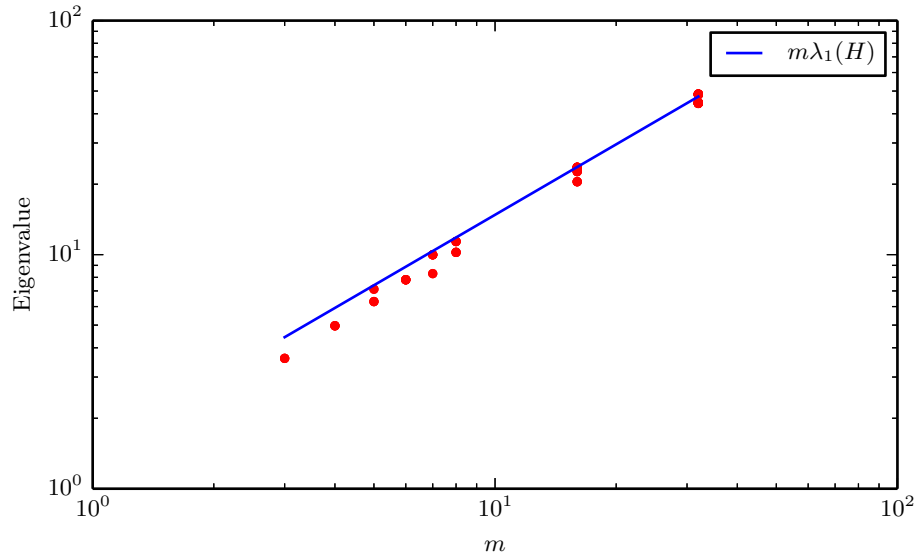


Figure 5: Plot of the eigenvalues at different values of  $m$ . The blue line is  $m\lambda_1(H)$  where  $H$  is the planar hexagon with area  $4\pi$  (equal to the surface area of the sphere).

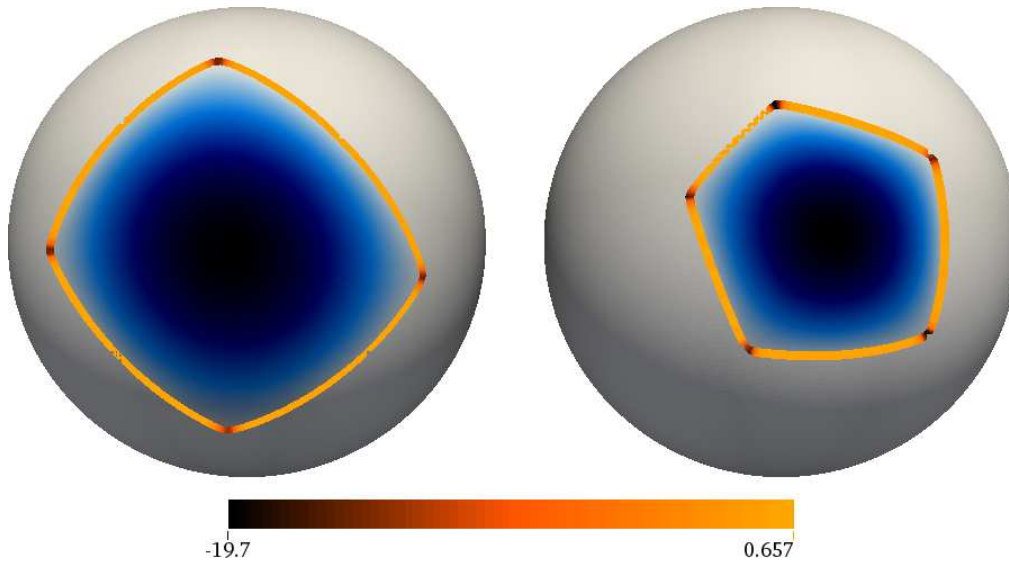


Figure 6: Plots of one partition and  $\kappa_g$  for  $m = 8$  (left) and  $m = 16$  (right). The value of  $u_i^{\varepsilon, h}$  is shown on a black to white scale and  $\kappa_g$  is plotted on the curve  $\{v_i^{\varepsilon, h} = 0\}$  on a black to orange scale.

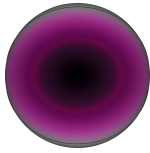
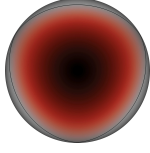
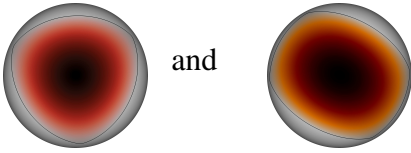
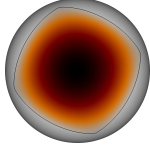
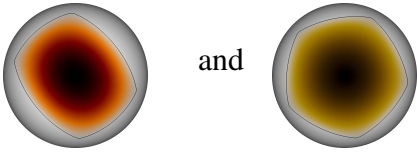
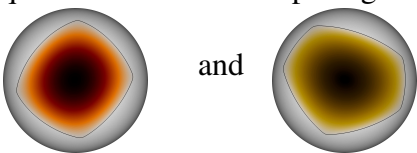
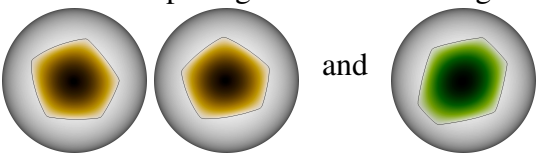
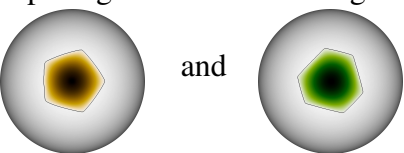
$m$	Shape	Energy information
3	3 lens 	Lens eigenvalue: $3.605 (2.59 \cdot 10^{-4})$ $S_\varepsilon$ : 0.072 Total energy: 10.887
4	4 triangles 	Triangle eigenvalue: $4.966 (2.46 \cdot 10^{-4})$ $S_\varepsilon$ : 0.121 Total energy: 19.987
5	2 triangles and 3 quadrilaterals 	Triangle eigenvalue: $7.118 (3.35 \cdot 10^{-4})$ Quadrilateral eigenvalue: 6.302 $S_\varepsilon$ : 0.187 Total energy: 33.330
6	6 quadrilaterals 	Quadrilateral eigenvalue: $7.812 (7.22 \cdot 10^{-4})$ $S_\varepsilon$ : 0.248 Total energy: 47.122
7	5 quadrilaterals and 2 pentagons 	Quadrilateral eigenvalue: $9.988 (1.63 \cdot 10^{-3})$ Pentagon eigenvalue: $8.298 (7.50 \cdot 10^{-5})$ $S_\varepsilon$ : 0.322 Total energy: 66.859
8	4 quadrilaterals and 4 pentagons 	Quadrilateral eigenvalue: $11.380 (5.31 \cdot 10^{-3})$ Pentagon eigenvalue: $10.230 (2.91 \cdot 10^{-3})$ $S_\varepsilon$ : 0.650 Total energy: 87.102
16	8 A and 4 B pentagons and 4 hexagons 	Pentagon (A) eigenvalue: $22.647 (1.05 \cdot 10^{-2})$ Pentagon (B) eigenvalue: $23.610 (2.43 \cdot 10^{-2})$ Hexagon eigenvalue: $20.496 (1.05 \cdot 10^{-2})$ $S_\varepsilon$ : 1.264 Total energy: 362.718
32	12 pentagons and 20 hexagons 	Pentagon eigenvalue: $48.436 (1.46 \cdot 10^{-1})$ Hexagon eigenvalue: $44.460 (1.24 \cdot 10^{-1})$ $S_\varepsilon$ : 2.496 Total energy: 1472.920

Table 3: More details of optimal partitions. In the small plots, we plot the corresponding  $u_i^{\varepsilon,h}$  with a black contour at  $v_i^{\varepsilon,h} = 0$ .



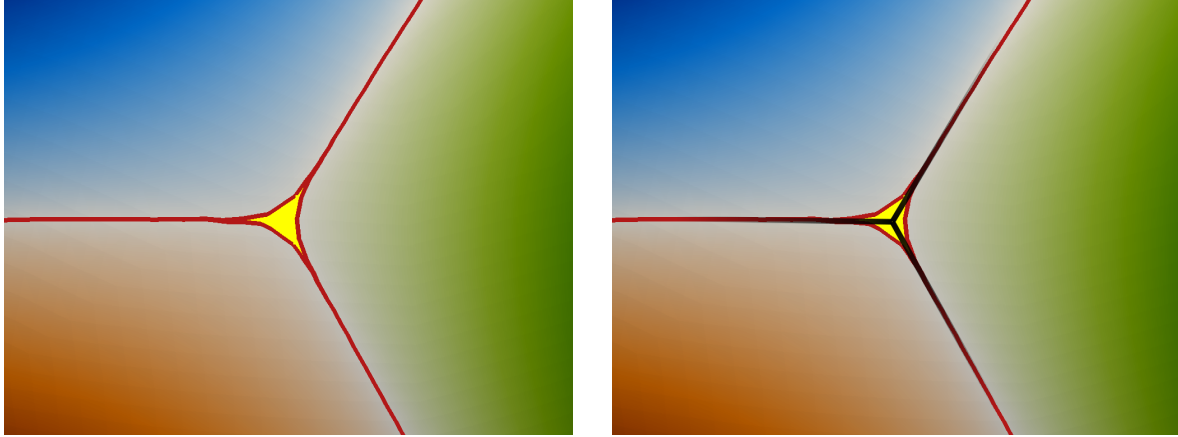


Figure 7: A zoom of a triple junction on the sphere. Three partitions  $\{v_i^{\varepsilon,h} > 0\}$  are coloured on blue, green and orange according to the eigenfunction  $u_i^{\varepsilon,h}$  with red boundaries at  $\{v_i^{\varepsilon,h} = 0\}$ . The void region is shown in yellow. Additionally in the right plot we have added black lines which would correspond to an equal angle triple junction.

- Each junction is a triple junction with an equal angle condition satisfied;
- There are at most two types of polygon in the partition;
- In the case of two different polygons, the polygon with more sides has lower eigenvalue;
- As  $m$  increases the number of edges in each polygon increases;
- Each polygon has at most 6 edges.

We define the dual polygon to a partition by considering the edges and vertices as a graph and taking the dual graph. In our case, since we always have triple junctions this defines a triangulation of the sphere. Let  $V$  be the number of vertices,  $E$  the number of edges and  $F$  the number of faces in the dual polygon to a partition  $\{\Gamma_i\}_{i=1}^m$ . We know that this will satisfy Euler's identity,  $V - E + F = \chi$ , where  $\chi$  is the Euler characteristic (2 in the case of a sphere), and also that

$$2E = \sum_{k=0}^{\infty} kn_k, \quad 3F = \sum_{k=0}^{\infty} kn_k, \quad V = \sum_{k=0}^{\infty} n_k,$$

where  $n_k$  is the degree of a vertex in the dual polygon. The degree of a vertex is equal to the number of edges of the corresponding partition. Using these equations in Euler's identity gives

$$4n_2 + 3n_3 + 2n_4 + n_5 = 6\chi + \sum_{k=7}^{\infty} (k-6)n_k. \quad (3.4)$$

This result is a special case of the Gauss-Bonnet theorem. We can think of this result as saying that polygons with less than six sides correspond to regions of positive Gauss curvature, hexagons

$m$	Surface ( $D$ )			Torus		
	$l$	Degrees of freedom	$\varepsilon$	$l$	Degrees of freedom	$\varepsilon$
3	12	311 982	$3.125 \cdot 10^{-4}$	12	393 216	$3.125 \cdot 10^{-4}$
4	12	415 976	$3.125 \cdot 10^{-4}$	12	524 288	$3.125 \cdot 10^{-4}$
5	10	256 365	$6.25 \cdot 10^{-4}$	10	326 680	$6.25 \cdot 10^{-4}$
6	9	150 900	$8.883 \cdot 10^{-4}$	10	393 216	$6.25 \cdot 10^{-4}$
7	9	176 050	$8.883 \cdot 10^{-4}$	10	458 752	$6.25 \cdot 10^{-4}$
8	9	201 200	$8.883 \cdot 10^{-4}$	10	524 288	$6.25 \cdot 10^{-4}$
16	9	402 400	$8.883 \cdot 10^{-4}$	10	1 048 576	$6.25 \cdot 10^{-4}$
32	9	804 800	$8.883 \cdot 10^{-4}$	8	1 045 696	$8.883 \cdot 10^{-4}$

Table 4: Final parameters for computations on the other surfaces ( $D$ ) and the torus.

correspond to zero Gauss curvature and polygons with more than six sides correspond to negative Gauss curvature.

This identity is consistent with the partitions in Table 3. Our computations suggest that the polygonal structure of the optimal partition consists of polygons with six or less sides. This agrees with the idea that the sphere has uniform positive Gauss curvature. We can deduce that if an  $m$ -partition of the sphere consists of only pentagons and hexagons, then there will be 12 pentagons and  $m - 12$  hexagons. We expect this to be the optimal partition for large values of  $m$ .

### 3.3 Computed partitions of other surfaces

We consider two other surfaces to see if these conclusions persist on a large class of surfaces. The first example, surface ( $D$ ), is taken from the work of Dziuk (1988) where the surface is given by  $\Gamma = \{x \in \mathbb{R}^3 : \Phi(x) = 0\}$  for  $\Phi$  given by

$$\Phi(x_1, x_2, x_3) := (x_1 - x_3^2)^2 + x_2^2 + x_3^2 - 1.$$

This has the same genus as a sphere but has large changes in curvature. The second example is given by a torus ( $T$ ) with inner radius 0.6 and outer radius 1. This has different genus to the sphere. We proceed with the same refinement strategy as on the sphere. Details of the parameters is given in Table 4.

We plot for the eigenvalues corresponding to the optimal partition Figure 8. We compute the eigenvalue as the  $H^1(\Gamma)$  semi-norm of each component. We have also included the line at  $m\lambda_1(H_D)$  and  $m\lambda_1(H_T)$  in each plot, where  $H_D$  and  $H_T$  are the regular hexagons with area equal to the surfaces of example 1 ( $D$ ) and the torus ( $T$ ). We do not have direct access to the eigenvalues on either of these surfaces so do not add that to this plot.

For surface ( $D$ ), we plot the optimal configurations in Figure 9 with more details given, including eigenvalues and energy, in Table 5. For the torus, we plot the optimal configurations in Figure 10 with more details given, include eigenvalues and energy, in Table 6.



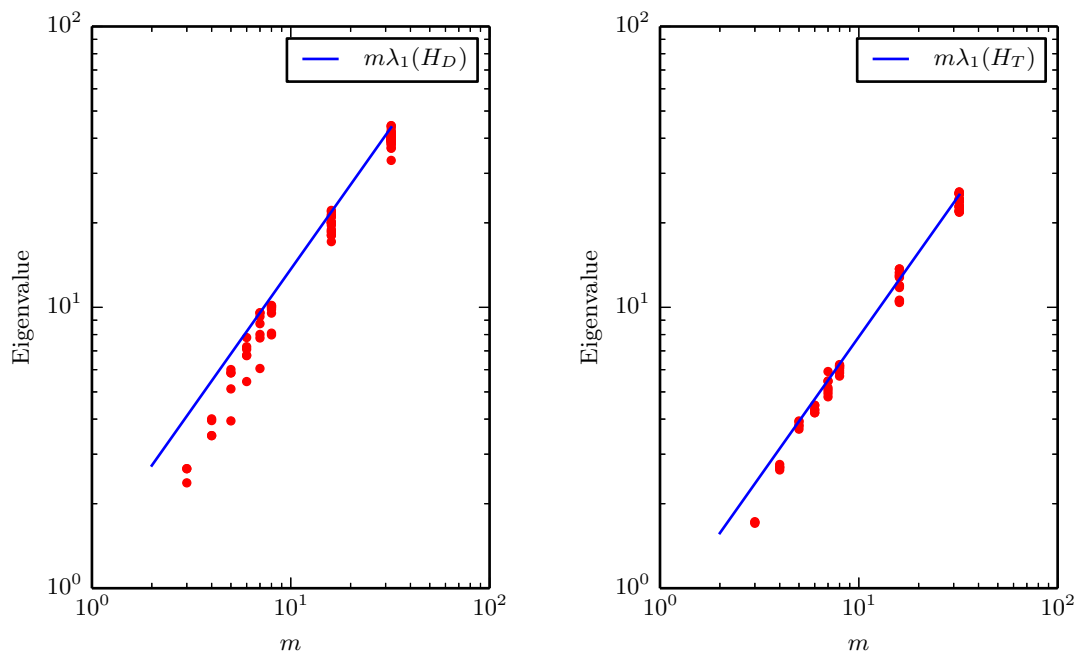


Figure 8: Plot of the eigenvalues at different values of  $m$ . Left for surface 1 ( $D$ ) and right for the torus ( $T$ ). The blue line indicates the scaled eigenvalue corresponding to a hexagon  $H$  of equal area to each surface – this is the conjectured average eigenvalue for large  $m$  in the plane (Caffarelli and Lin 2007).

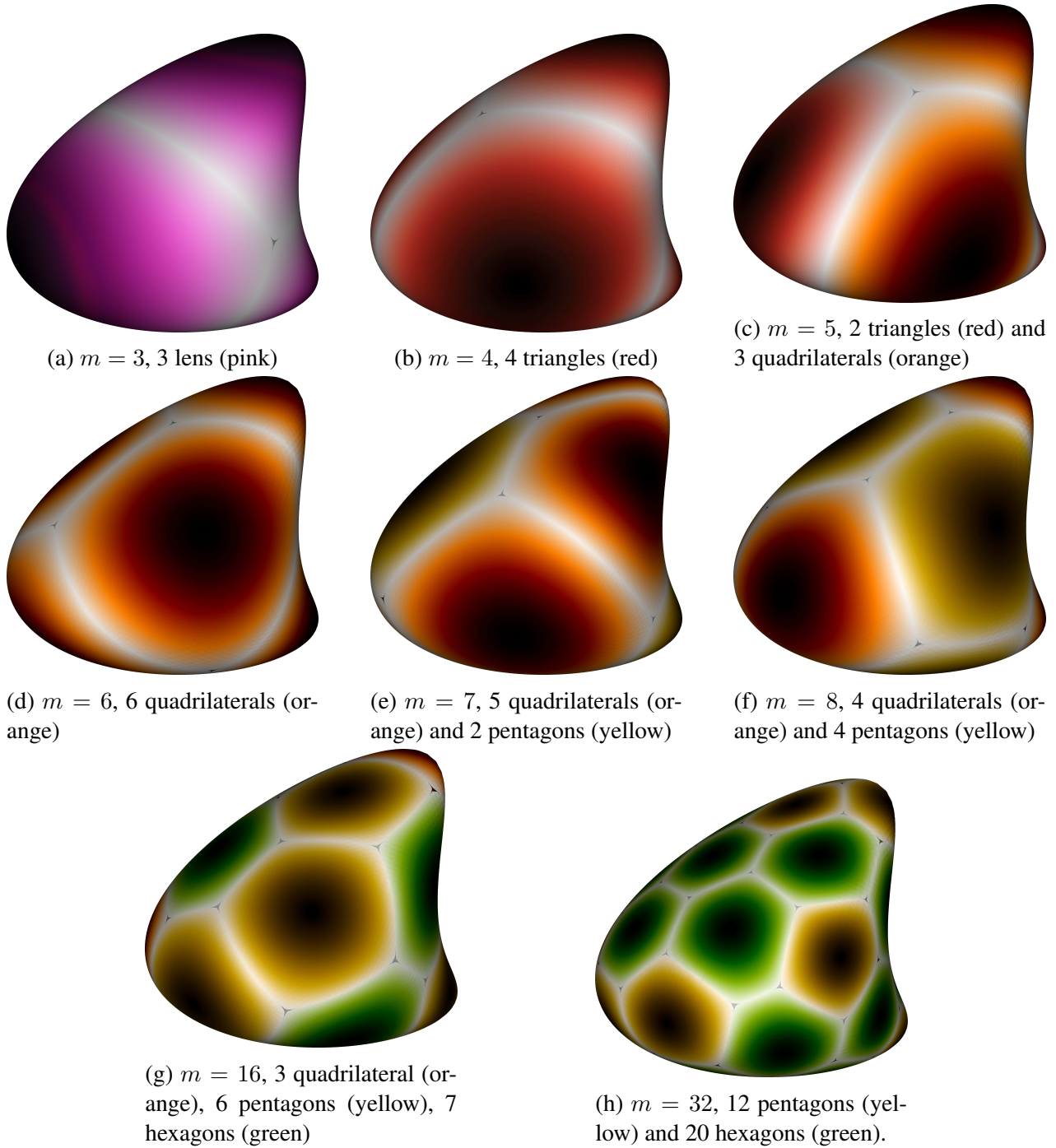


Figure 9: Plots of the minimising configurations on the example surface one. Same colouring as Figure 4

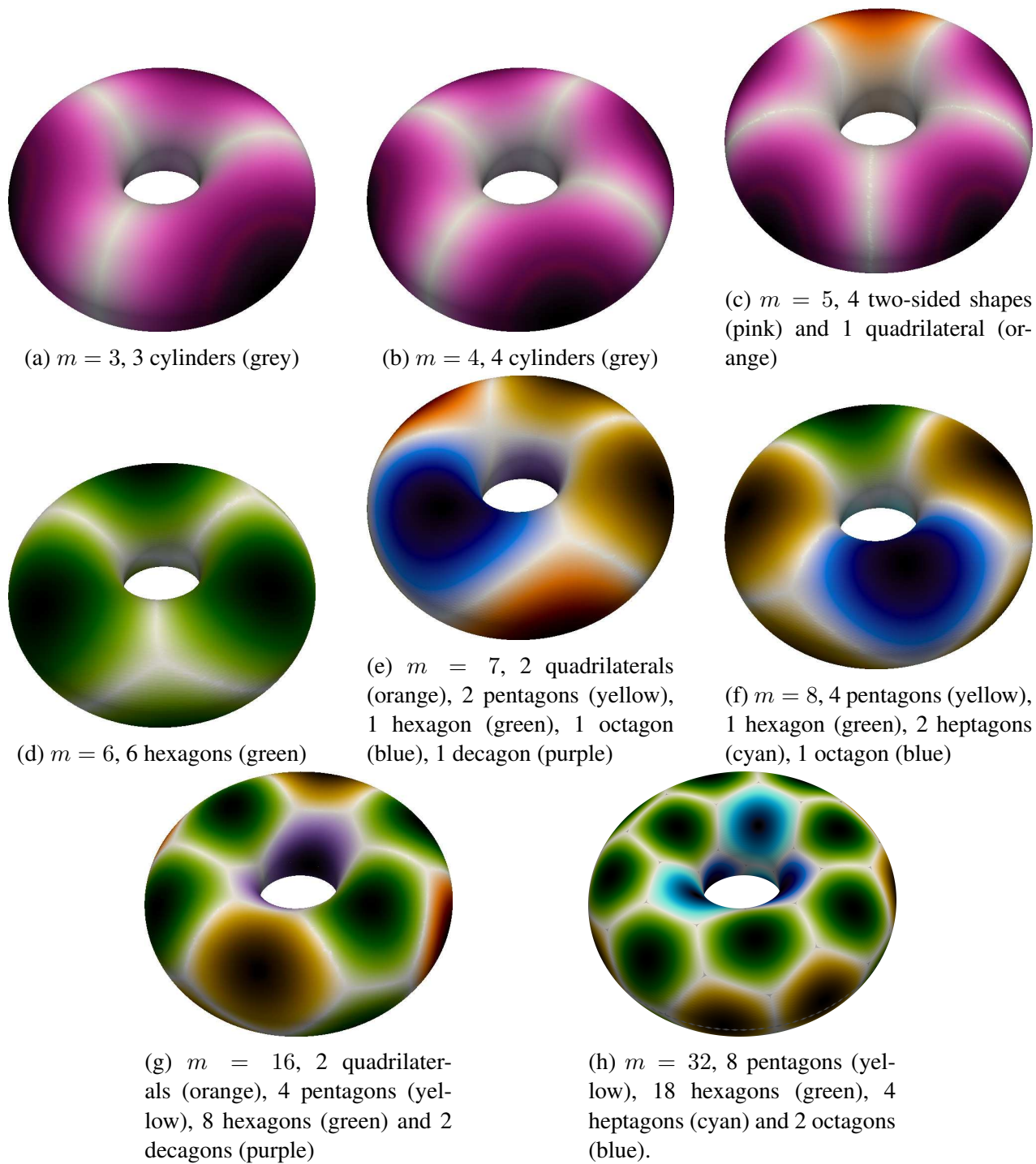
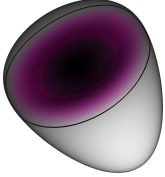
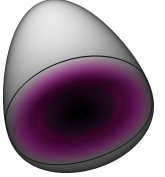
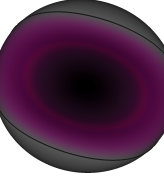
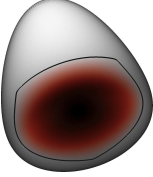
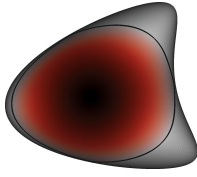
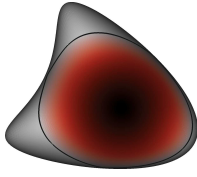
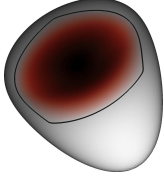
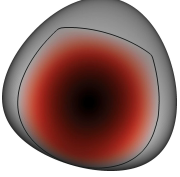
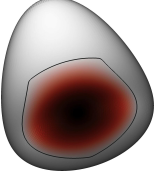
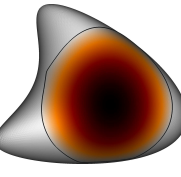
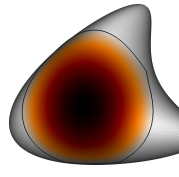
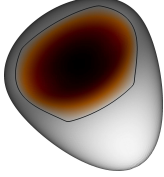
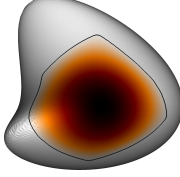
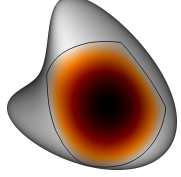
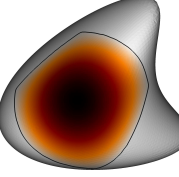
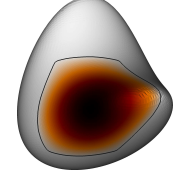
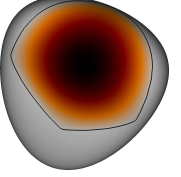
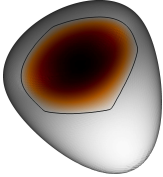


Figure 10: Plots of the minimising configurations on the torus. Same colouring as Figure 4

$m$	Partition				
3	lens		crescent	crescent	
					
	2.664		2.664	2.372	
	$S_\varepsilon: 0.040$				
	Total energy: 7.741				
4	triangle	triangle	triangle	triangle	
					
	3.493	3.494	4.008	3.952	
	$S_\varepsilon: 0.103$				
	Total energy: 15.051				
5	triangle	triangle	quadrilateral	quadrilateral	quadrilateral
					
	5.843	5.125	6.004	5.944	3.942
	$S_\varepsilon: 0.312852$				
	Total energy: 27.072				
6	quadrilateral	quadrilateral	quadrilateral	quadrilateral	quadrilateral
					
	7.808	7.241	7.093	6.753	6.730
	quadrilateral				
					
	5.443				
	$S_\varepsilon: 0.753$				
	Total energy: 41.821				

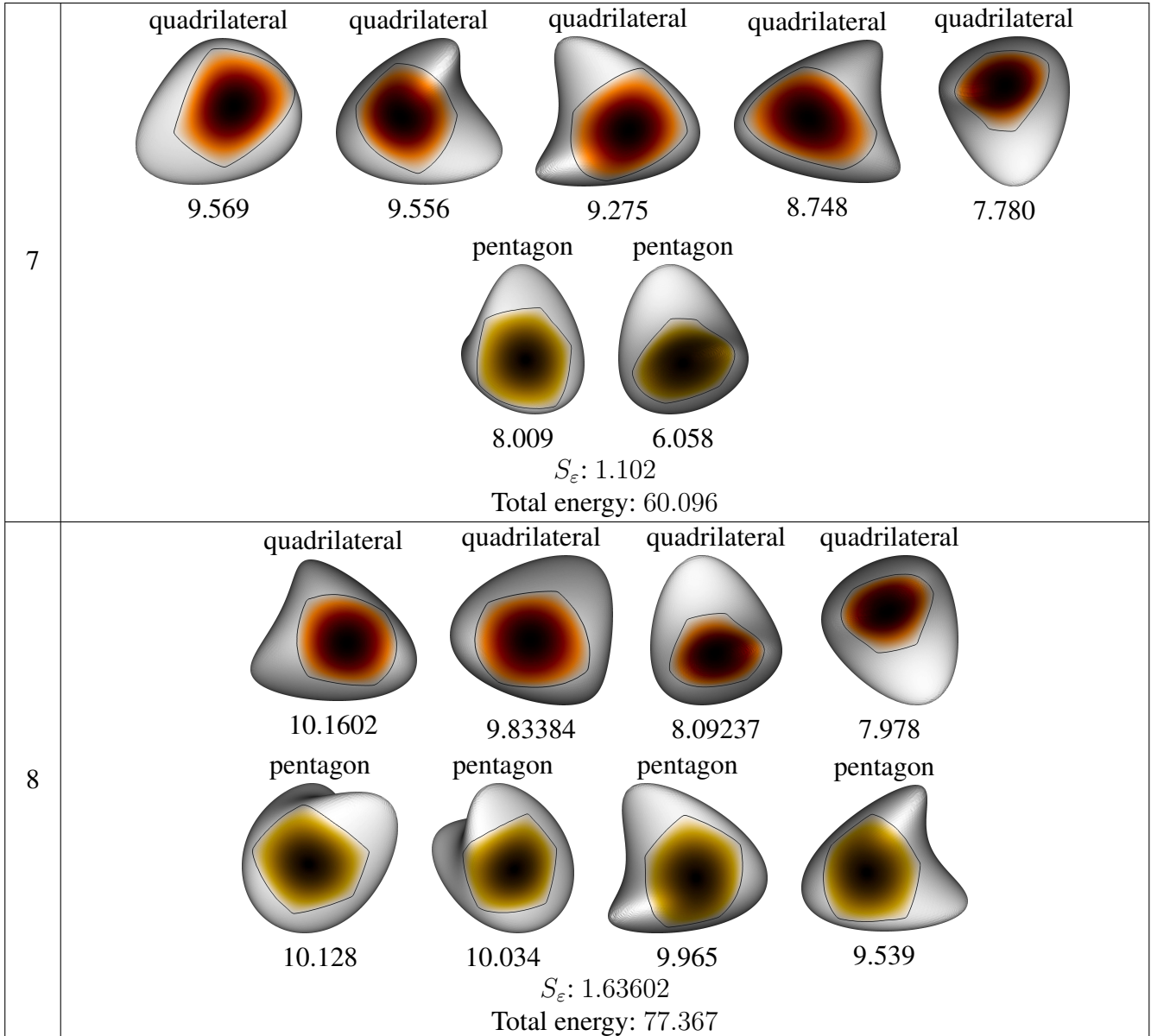
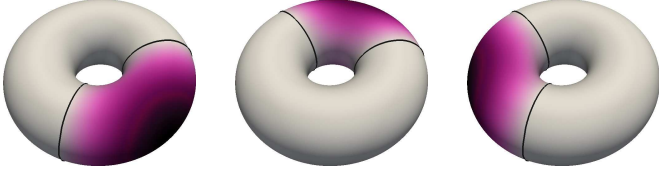
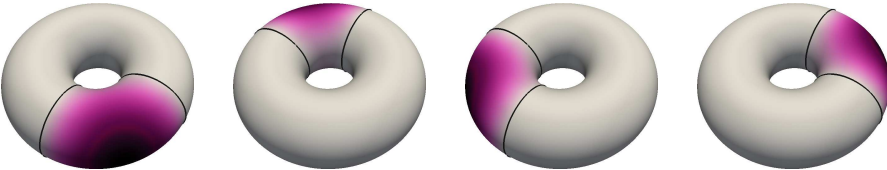
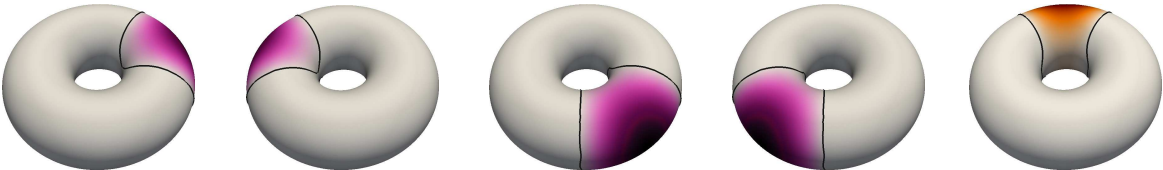
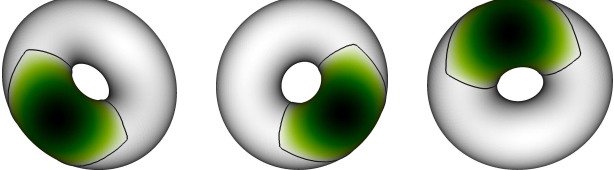
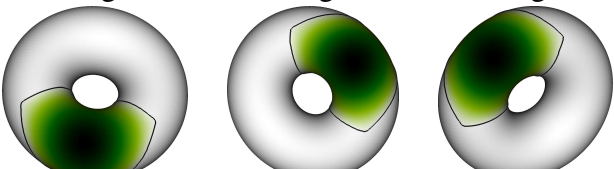


Table 5: More details of optimal partitions. In the small plots, we plot the corresponding  $u_i^{\varepsilon,h}$  with a black contour at  $v_i^{\varepsilon,h} = 0$ .



$m$	Partition				
3	<p>cylinder      cylinder      cylinder</p>  <p>1.725      1.703      1.717</p> <p><math>S_\varepsilon</math>: 1.207</p> <p>Total energy: 6.353</p>				
4	<p>cylinder      cylinder      cylinder      cylinder</p>  <p>2.758      2.637      2.595      2.595</p> <p><math>S_\varepsilon</math>: 0.106</p> <p>Total energy: 10.890</p>				
5	<p>two sided shape      two sided shape      two sided shape      two sided shape      quadrilateral</p>  <p>3.772      3.940      3.683      3.914      3.812</p> <p><math>S_\varepsilon</math>: 0.595</p> <p>Total energy: 19.717</p>				
6	<p>hexagon      hexagon      hexagon</p>  <p>4.215      4.481      4.319</p> <p>hexagon      hexagon      hexagon</p>  <p>4.319      4.480      4.215</p> <p><math>S_\varepsilon</math>: 1.005</p> <p>Total energy: 27.035</p>				

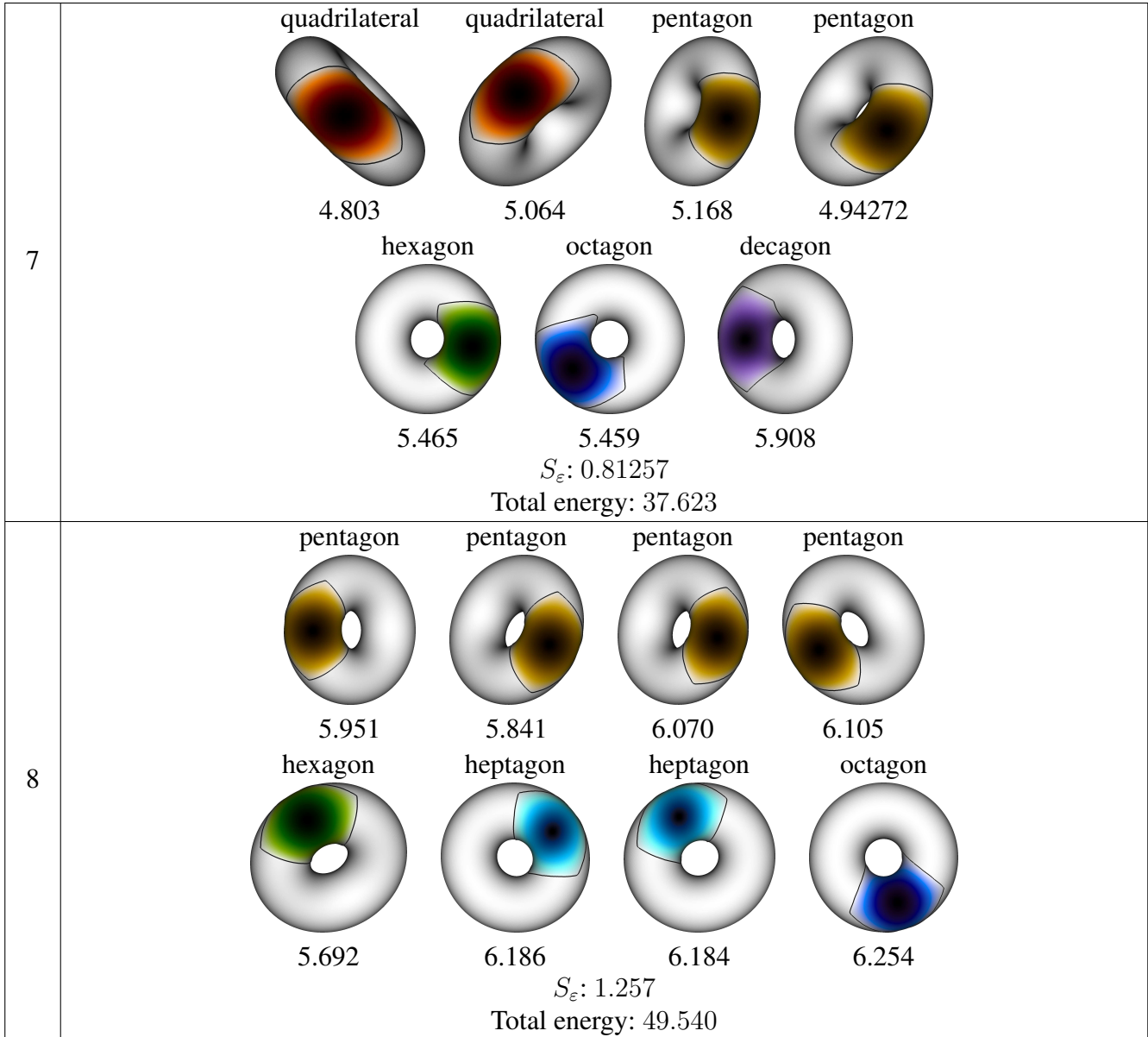


Table 6: More details of optimal partitions. In the small plots, we plot the corresponding  $u_i^{\varepsilon,h}$  with a black contour at  $v_i^{\varepsilon,h} = 0$ .

By using  $\Gamma_i^{\varepsilon,h}$  and  $v_i^{\varepsilon,h}$  from (3.2), we can define the boundary of partition on these surfaces also. This allows us to compute the geodesic curvature (3.3) of the boundary of  $\Gamma_i^{\varepsilon,h}$ ; see Figure 11 for computations. We again see that away from junctions the geodesic curvature is small. We also see that boundaries all meet at triple junction with the equal angle condition satisfied. We conjecture that on all surfaces optimal partitions have boundaries with zero geodesic curvature which meet at triple junctions with equal angles between each boundary.

On surface ( $D$ ), the partition has exactly the same structure as for the sphere for  $m \leq 8$  but the eigenvalues do not group in the same way because of the variations in curvature. For large values of  $m$  the structure changes. Now in regions with higher curvature we see partitions with few sides. In fact, for  $m = 16$ , three partitions have four sides, which does not occur in the case of the sphere. The familiar pattern of pentagons and hexagons reoccurs for  $m = 32$  except now the pentagons are clustered in regions of high curvature. The number of sides of each partition is still limited to six. Because of (3.4), for larger values of  $m$  we expect to see 12 pentagons and  $m - 12$  hexagons with the pentagons clustered in the higher curvature regions.

On the torus, example ( $T$ ), the situation is very different. For  $m \leq 6$ , we have very structured partitions which reflect the symmetry of the surface. For the case of  $m = 5$ , we see all triple junctions occur in the center of the torus. For  $m > 6$ , we have partitions with more than 6 sides. The formula (3.4) tells us that the numbers of partitions with more than six sides must balance the number of partitions with less than six sides. For the cases we see, the partitions with more than six sides cluster in the center and those with less than six sides cluster on the exterior. As we increase  $m$  we see an increase in the number of hexagons, and it is not clear whether the number of partitions with different to six sides will decrease. For smaller area partitions, for larger  $m$ , the curvature of the surface is less important and the problem becomes more like the flat problem, so we expect that for large values of  $m$ , we will see a preponderance of hexagons.

## 4 Discussion

We have explored an eigenvalue partition problem on three different surfaces and for many different numbers of partitions. We have observed good convergence both with respect to discretisation parameters and also with respect to our choice of regularisation. From our results we make the following conjectures:

1. The optimal partition consists of curvilinear polygons whose edges have zero geodesic curvature.
2. Partitions either meet along edges or at triple junctions where edges meet at equal angles.
3. For genus zero surfaces, for large values of  $m$  the optimal partition consists of 12 pentagons and  $m - 12$  hexagons. If the curvature of the surface varies, the pentagons will be located where the curvature is highest.



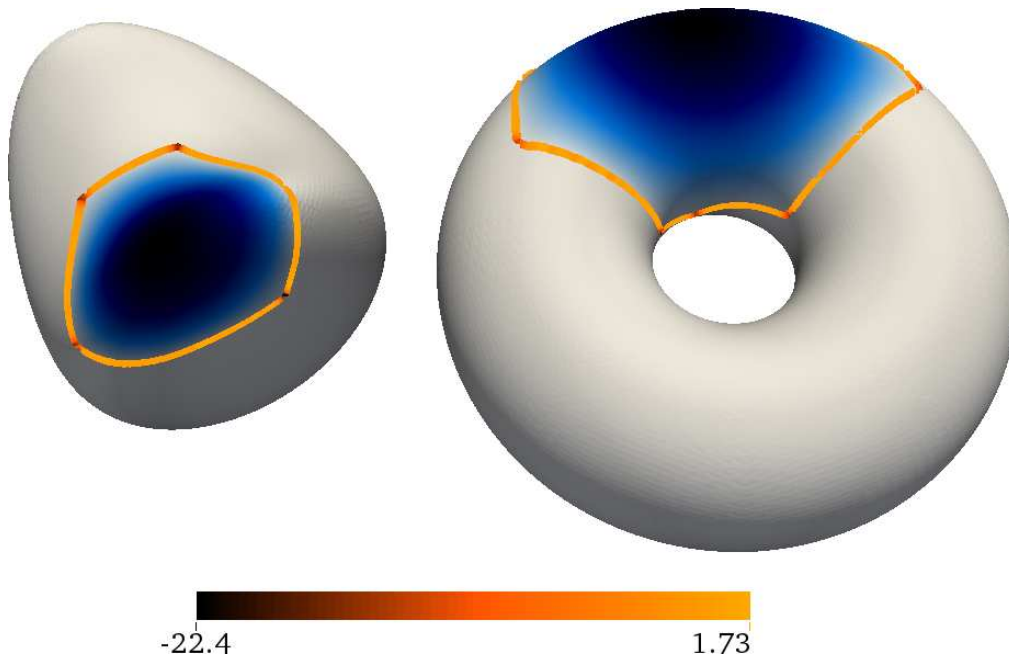


Figure 11: Plots of one partition and  $\kappa_g$  for  $m = 8$  for Example 1 (left) and  $m = 6$  for Example 2 (right). The value of  $u_i^{\varepsilon,h}$  is shown on a black to white scale and  $\kappa_g$  is plotted on the curve  $\{v_i^{\varepsilon,h} = 0\}$  on a black to orange scale.

4. For genus one surfaces, for large values of  $m$  the optimal partition has a preponderance of hexagons.

## Acknowledgments

The research of TR was funded by the EPSRC (grant number EP/L504993/1). This work was undertaken on ARC2, part of the High Performance Computing facilities at the University of Leeds. The authors were participants of the Isaac Newton Institute programme Free Boundary Problems and Related Topics (January–July 2014) when this article was written.

## References

- Bao, W. and Du, Q. Computing the ground state solution of Bose–Einstein condensates by a normalized gradient Flow. *SIAM J. Sci. Comput.*, 25(5):1674–1697, 2004.
- Bastian, P., Blatt, M., Dedner, A., Engwer, C., Klöforn, R., Kornhuber, R., Ohlberger, M., and Sander, O. A generic grid interface for parallel and adaptive scientific computing. Part II: implementation and tests in DUNE. *Comput.*, 82(2–3):121–138, 2008a.
- Bastian, P., Blatt, M., Dedner, A., Engwer, C., Klöforn, R., Ohlberger, M., and Sander, O. A

- generic grid interface for parallel and adaptive scientific computing. Part I: abstract framework. *Comput.*, 82(2–3):103–119, 2008b.
- Blatt, M. and Bastian, P. The iterative solver template library. In *Proceedings of the 8th international conference on Applied parallel computing: state of the art in scientific computing*, PARA'06, pages 666–675, Berlin / Heidelberg, 2007. Springer-Verlag.
- Bonnaillie-Noël, V., Helffer, B., and Vial, G. Numerical simulations for nodal domains and spectral minimal partitions. *ESAIM: Control Optim. Calc. Var.*, 16:221–246, 1 2010.
- Bourdin, B., Bucur, D., and Oudet, E. Optimal partitions for eigenvalues. *SIAM J. Sci. Comput.*, 31(6):4100–4114, 2010.
- Bozorgnia, F. Numerical algorithm for spatial segregation of competitive systems. *SIAM J. Sci. Comput.*, 31(5):3946–3958, 2009.
- Bozorgnia, F. and Arakelyan, A. Numerical algorithms for a variational problem of the spatial segregation of reaction–diffusion systems. *Appl. Math. Comput.*, 219(17):8863 – 8875, 2013.
- Bucur, D. and Zolesio, J. N-dimensional shape optimization under capacitary constraint. *J. Differ. Equations*, 123(2):504 – 522, 1995.
- Bucur, D., Buttazzo, G., and Henrot, A. Existence results for some optimal partition problems. *Adv. Math. Sci. Appl.*, 8:571–579, 1998.
- Buttazzo, G. and Dal Maso, G. An existence result for a class of shape optimization problems. *Arch. Ration. Mech. An.*, 122(2):183–195, 1993.
- Caffarelli, L. and Lin, F. An optimal partition problem for eigenvalues. *J. Sci. Comput.*, 31(1-2): 5–18, 2007.
- Caffarelli, L. and Lin, F. Singularly perturbed elliptic systems and multi-valued harmonic functions with free boundaries. *J. Am. Math. Soc.*, 21(3):847–862, 2008.
- Caffarelli, L. and Lin, F. Nonlocal heat flows preserving the  $L^2$  energy. *Discrete Cont. Dyn. – A*, 23:49–64, 2009.
- Chang, S. M., Lin, C. S., Lin, T. C., and Lin, W. W. Segregated nodal domains of two-dimensional multispecies Bose-Einstein condensates. *Phys. D.*, 196(3–4):341–361, 2004.
- Chen, L.-Q. Phase-field models for microstructure evolution. *Annu. Rev. Mater. Res.*, 32:113–140, 2002.
- Coifman, R. R. and Lafon, S. Diffusion maps. *Appl. Comput. Harmon. A.*, 21(1):5 – 30, 2006.

- Conti, M., Terracini, S., and Verzini, G. Nehari's problem and competing species systems. *Ann. I. H. Poincaré – AN*, 19(6):871 – 888, 2002.
- Conti, M., Terracini, S., and Verzini, G. An optimal partition problem related to nonlinear eigenvalues. *J. Funct. Anal.*, 198(1):160 – 196, 2003.
- Conti, M., Terracini, S., and Verzini, G. Asymptotic estimates for the spatial segregation of competitive systems. *Adv. Math.*, 195(2):524 – 560, 2005a.
- Conti, M., Terracini, S., and Verzini, G. A variational problem for the spatial segregation of reaction-diffusion systems. *Indiana Univ. Math. J.*, 54:779–816, 2005b.
- Dedner, A., Klöforn, R., Nolte, M., and Ohlberger, M. A generic interface for parallel and adaptive discretization schemes: abstraction principles and the DUNE-FEM module. *Comput.*, 90(3-4): 165–196, 2010.
- Du, Q. and Lin, F. Numerical approximations of a norm-preserving gradient flow and applications to an optimal partition problem. *Nonlin.*, 22(1):67, 2009.
- Dziuk, G. Finite Elements for the Beltrami operator on arbitrary surfaces. In Hildebrandt, S. and Leis, R., editors, *Partial Differential Equations and Calculus of Variations*, volume 1357 of *Lecture Notes in Mathematics*, pages 142–155. Springer-Verlag, Berlin, 1988.
- Dziuk, G. and Elliott, C. M. Surface finite elements for parabolic equations. *J. Comp. Math.*, 25(4): 385–407, 2007.
- Dziuk, G. and Elliott, C. M. Finite element methods for surface PDEs. *Acta Numer.*, 22:289–396, 2013.
- Gräser, C., Kornhuber, R., and Sack, U. Nonsmooth Schur–Newton methods for multicomponent Cahn–Hilliard systems. *IMA Journal of Numerical Analysis*, 2014.
- Helfffer, B., Hoffmann-Ostenhof, T., and Terracini, S. On spectral minimal partitions: the case of the sphere. In Laptev, A., editor, *Around the Research of Vladimir Maz'ya III*, volume 13 of *International Mathematical Series*, pages 153–178. Springer New York, 2010.
- Henderson, A. ParaView: Parallel visualization application (Version 4.1.0) [Computer Software]. Available at <http://www.paraview.org>, 2014.
- Mayer, U. F. Gradient flows on nonpositively curved metric spaces and harmonic maps. *Commun. Anal. Geom.*, 6(2):199–253, 1998.
- Osting, B., White, C. D., and Oudet, E. Minimal Dirichlet energy partitions for graphs. *arXiv*, 1308.4915, 2014.
- Sverak, V. On optimal shape design. *J. Math. Pure Appl.*, 72:537–551, 1993.